A dual wavelength distributed-feedback fiber laser

AIP | Journal of Applied Physics

A dual wavelength distributed-feedback fiber laser

Nathaniel Groothoff, Cicero Martelli, and John Canning

Citation: Journal of Applied Physics **103**, 013101 (2008); doi: 10.1063/1.2826748
View online: http://dx.doi.org/10.1063/1.2826748
View Table of Contents: http://scitation.aip.org/content/aip/journal/jap/103/1?ver=pdfcov
Published by the AIP Publishing

A dual wavelength distributed-feedback fiber laser

Nathaniel Groothoff[a)]
Interdisciplinary Photonics Laboratories, School of Chemistry, The University of Sydney, 206 NIC, ATP, Sydney, NSW 1430, Australia, and School of Physics, The University of Sydney, Sydney, NSW 2006, Australia

Cicero Martelli
Interdisciplinary Photonics Laboratories, School of Chemistry, The University of Sydney, 206 NIC, ATP, Sydney, NSW 1430, Australia and School of Electrical and Information Engineering, The University of Sydney, Sydney, NSW 2006, Australia

John Canning
Interdisciplinary Photonics Laboratories, School of Chemistry, The University of Sydney, 206 NIC, ATP, Sydney, NSW 1430, Australia

(Received 13 September 2007; accepted 23 October 2007; published online 2 January 2008)

An approach to accessing air holes in a structured optical fiber with a distributed-feedback (DFB) laser based on higher order mode lasing is proposed and demonstrated. A narrow linewidth DFB fiber laser is fabricated in rare-earth-doped structured optical fiber. A higher order mode is shown to lase. Dual laser operation in both fundamental and higher order modes is also achieved. Numerical simulation of the mode profiles within the fiber using the adjustable boundary conditions-Fourier decomposition method supports the experimental results. Laser performance for each mode is characterized including imaging the emission of pump and lasing mode intensity profiles. © *2008 American Institute of Physics*. [DOI: 10.1063/1.2826748]

I. INTRODUCTION

The first reports of a distributed-feedback (DFB) resonant cavity generating laser emission were in 1971 by Kogelnik *et al.*[1] and Kaminow *et al.*[2] Both devices were based on dye lasers. Room-temperature distributed-feedback (DFB) semiconductor lasers based on InGaAsP/InP operating in the near-infrared (1.3–1.5 μm) region were developed in 1981.[3,4] It was not until 1994 when the first complex fiber grating, a phase-shifted structure designed for DFB fiber lasers, was demonstrated[5] that fiber DFB lasers became possible. Although there were unpublished demonstrations of these lasers as well as reported structures that were unlikely to be DFB action, the first reported DFB fiber laser that was unambiguously a distributed-feedback structure, which also employed UV-postprocessing, was by Asseh *et al.*[6] Since this development, the field of research in DFB fiber lasers has been extensive.[7–9]

The phase-shifted DFB structure is usually an UV-written Bragg grating with an induced phase shift at or near the center. For fiber-based DFB lasers the easiest method to introduce the phase shift is through a localized refractive index change arising from exposure to UV light.[5,10] DFB structures written with UV light sources operating below the damage threshold in a one-photon regime access particular defects in the glass and lead to polarizability changes caused by defect formation and destruction as well as some densification.[11] In the absence of sufficient defect sites for UV absorption, hydrogen can be dissolved into the fiber to introduce absorption sites, most likely through hydride formation.[12] However, hydrogen can introduce losses in optical waveguides through OH formation when exposed to UV light[13]—these can be significantly reduced by using hypersensitization.[14,15] Another promising technique is to use high-intensity UV light to accesses the band edge of silica, ~(140–157)nm, through a two-photon initiated process[16,17]—this means photosensitive dopants are not necessary. An apparent advantage of adding rare-earth dopants into the fiber is the increased efficiency of FBG production while still avoiding the requirement of hydrogen or hypersensitization.

The attractiveness of DFB devices stems from inherent properties that permit numerous applications. They incorporate a narrow linewidth,[7,9,18] leading to an increase in the number of channels in a wavelength division multiplexed system. Dual or single polarization lasing[19–21] can occur depending on a fiber's inherent birefringence as well as external geometrical influences: for example, twisting the DFB either prior to or after the grating inscription. Polarization can be used in sensing applications that change the fiber's birefringence.

The first solid core with air cladding fiber for optical guidance was developed by Kaiser *et al.*[22] Interest in this type of fiber was not renewed until Knight *et al.*[23] developed optical fibers consisting of a cladding made from a series of holes periodically positioned, running coaxially with the fiber, situated around a central solid core, a defect where there is a missing hole. These air-silica structured fibers, also known as photonic crystal fibers, were developed to study photonic crystal guidance over an extended length that was unachievable using conventional two-dimensional planar devices. The confinement properties can exist in different forms: (1) guidance through an effective total-internal

[a)]Author to whom correspondence should be addressed. Electronic mail: n.groothoff@usyd.edu.au.

reflection,[24] although even in these fibers there is diffractive guidance at short wavelengths,[25] and (2) confinement from coherent scattering, the so-called band-gap effect,[26–29] which has also been proposed and demonstrated with the refractive index changes located at the Fresnel zones.[30,31] The reliance on the holes for mode confinement in conjunction with large index contrast means that modification to the confinement and waveguiding properties can be achieved by altering the configuration and size of the holes.[24,32] Geometrical alteration of the holes, whether through holes size or size and shape of the solid core, readily creates waveguides of large birefringence.[33,34]

As the confinement is controlled by the holes, a percentage of the mode propagates inside the hole. The shape and position of the holes can be used to tailor the stress-optic coefficient of the fibers.[35] Any material that is inserted into the holes will ultimately alter the effective index of the mode—this has been used to change the macroproperties of the fiber, including thermo-optic coefficient.[36] In this case, the possibility of creating strain-free temperature-independent gratings in structured fibers is possible. Numerous sensing applications have been demonstrated.[37–39] By doping the core of air-silica structured fibers with germanium, improved dispersion characteristics were achieved[40] showing larger customization. Germanium doping in the core allowed Bragg gratings to be written,[41] although some of the advantages of the structured fiber, particularly the evanescent field extending into the holes, are lost. Core cladding interactions also become problematic. To overcome these limitations of conventional grating writing, we demonstrated gratings in pure silica fiber.[17] No core cladding interactions are observed with little compromise on the evanescent field penetration into the holes. For DFB laser applications, germanium is often not wanted and the ability to write gratings in germanium-free fibers, both step index and photonic crystal, becomes important. Similarly, other dopants, such as rare earths, can be added to air-silica structured fibers, creating active devices. The concept of a distributed-feedback fiber laser produced in a photonic crystal fiber was theoretically analyzed by Søndergaard.[42] Amplification properties of rare-earth doped photonic crystal fiber were also examined,[43] demonstrating improvements beyond that of conventional step-index fibers. The possibility of exploiting band-gap properties of the crystal structure and the laser characteristics, including potentially reduced amplified spontaneous emission, is of great fundamental interest.

The first demonstration of an erbium-doped air-silica structured fiber laser used a distributed Bragg reflector to form the resonant cavity.[44] Subsequent to this development, a distributed-feedback fiber laser was fabricated in the same erbium-doped air-silica structured fiber (ASSF).[45] The process of grating inscription required a high-intensity deep UV laser (Exciplex ArF 193 nm) since the photosensitivity of the fiber was low because we wanted to avoid both germanium and hydrogen sensitization. The DFB-PCF device showed single-mode operation and preliminary studies showed narrow linewidth operation ($\Delta\lambda < 50$ kHz). However, from a sensing perspective it suffered the problem we raised above—the dopants created a step-index profile that saw the field confined within the core more efficiently than if there were no dopants, reducing possible interactions. A smaller core is drawn to partially overcome this. It is extremely challenging to overcome the step index using complex dopant formulations to offset the raised index. Significant developmental engineering and cost is required to work toward this.

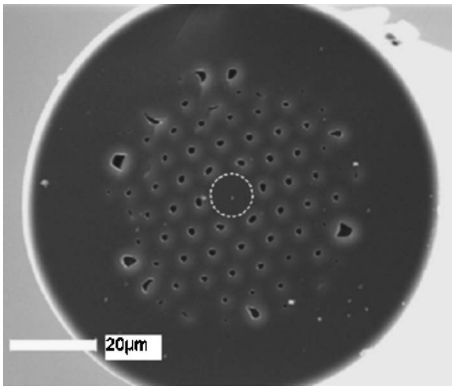

FIG. 1. SEM end face cross section of the Er^{3+}-doped ASSF. Erbium region shown by dash circle.

In this paper we propose an alternative approach to improve access to the holes of the DFB laser for sensing applications. We present selective lasing from an erbium-doped core ASSF with a DFB structure produced using similar methods we reported for single-mode operation.[45] Numerical simulation of the waveguide showed that the erbium-doped region is capable of supporting two modes at the laser wavelength (1530 nm) and, subsequently, at the pump wavelength (976 nm), which was experimentally verified. The higher order mode has significantly enhanced interaction with the holes. Further, another advantage exists if lasing on both modes is possible—the ability to analyze differences between the two modes and deduce influences from a material inserted into the holes. Since the higher order mode interacts with the hole structure far more than the fundamental mode, it can be used as the sensing probe, while the fundamental mode can be used as the reference signal. Built into such a system would be the ability to separate out temperature and strain effects.

II. FIBER FABRICATION AND GRATING WRITING

The generic stack and draw method was used to fabricate the doped core ASSF. The erbium-aluminosilicate core was fabricated by modified chemical vapor deposition (MCVD)[44,45] and solution doping process. The addition of aluminum is to reduce erbium clustering.[46] This, however, is the main source raising the refractive index which produces the step-index properties alluded to above. For stacking, the erbium-doped preform's diameter was etched down to capillary dimensions using hydrofluoric acid. After stacking, the perform was drawn into fiber using a conventional fiber drawing process. Figure 1 displays a scanning electron micrograph of the end face of the fiber with a diameter of 100 μm. Additional information regarding the fabrication of the fiber can be found in Ref. 44.

Dual mode operation was previously observed from the distributed Bragg reflector (DBR) laser, comprised of two 1

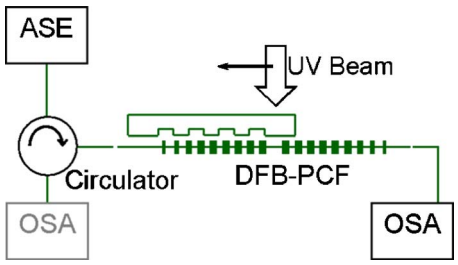

FIG. 2. (Color online) Schematic of UV grating direct writing configuration. ASE: amplified spontaneous emission from erbium-doped fiber amplifier, OSA: optical spectrum analyzer.

cm long fiber Bragg gratings, separated by 17 cm, written into the doped ASSF.[44] The authors attribute the dual modes to the combined structure of the Er^{3+} core and the silica ring surrounding the Er^{3+} both acting as a waveguide with different effective indices. On the other hand, a DFB laser[45] fabricated in a similar fashion showed single transverse and longitudinal mode operation, although in both orthogonal polarization eigenstates. The origin of the polarization arose from either the asymmetry in the core or the air-silica lattice, asymmetry in the Bragg grating itself, pump polarization selecting out aligned defects, or a combination of the causes.

The present DFB was fabricated using the same method as the previous DFB laser,[45] where a high-intensity process, initiated by two-photon absorption but driven by rare earth (and possibly transient defect) assisted coupling into the glass matrix. A GSI Lumonics UV exciplex laser (ArF, 193 nm, 15 ns pulse width) was used to write two 50 mm gratings separated by a phase shift cavity 1 mm wide with a pulse energy of 300 mJ/cm^2 up to a cumulative fluence of 5 kJ/cm^2. In contrast to pure silica gratings, the transient excitation through the rare earths greatly reduces the required fluence for writing gratings. Fine tuning of the phase shift with UV postprocessing was done subsequent to writing. Figure 2 displays the writing schematic for the gratings. To allow handling and coupling, lengths of approximately 20 mm were left on either side of the DFB structure. Grating characterization was done using the amplified spontaneous emission (ASE) from an erbium-doped fiber amplifier and optical spectrum analyzer (OSA resolution: 50 pm) through butt-coupling conventional fiber (single mode 1550 nm) to the ASSF. By adjusting the coupling conditions and hence mode excitation, selective characterization of both modes was achieved [Fig. 3(a)]. The fundamental mode had a Bragg wavelength $\lambda_B(f)=1531.55$ nm while for the high-order mode it was $\lambda_B(\text{ho})=1527.70$ nm. To allow direct comparison between the different characterization and analysis spectra (FBG spectra, high-resolution spectra, and lasing spectra), the wavelength scale was changed from absolute wavelength to relative detuning by normalizing the wavelength shift to the fundamental mode (i.e., 1531.55 nm$\rightarrow$0 nm). The feature located at −2 nm is cross coupling between the two modes, an artifact inherent when Bragg gratings are written in multimode fibers.[48]

The resolution of the OSA was insufficient to resolve the phase shift; therefore, a high-resolution spectrum of the fundamental mode was recorded [Fig. 3] using a swept wavelength source and power meter. The swept wavelength source had a noise floor of ~−15 dB; this prevented some features of the grating and phase shift from being observed. To estimate the strength of the grating, a numerical simulation by transfer matrix methods was used which indicated a grating strength in excess of 100 dB, assuming uniform periodic refractive index profile over 100 mm length and modal confinement by the step-index region of the fiber (see Fig. 3(b)).

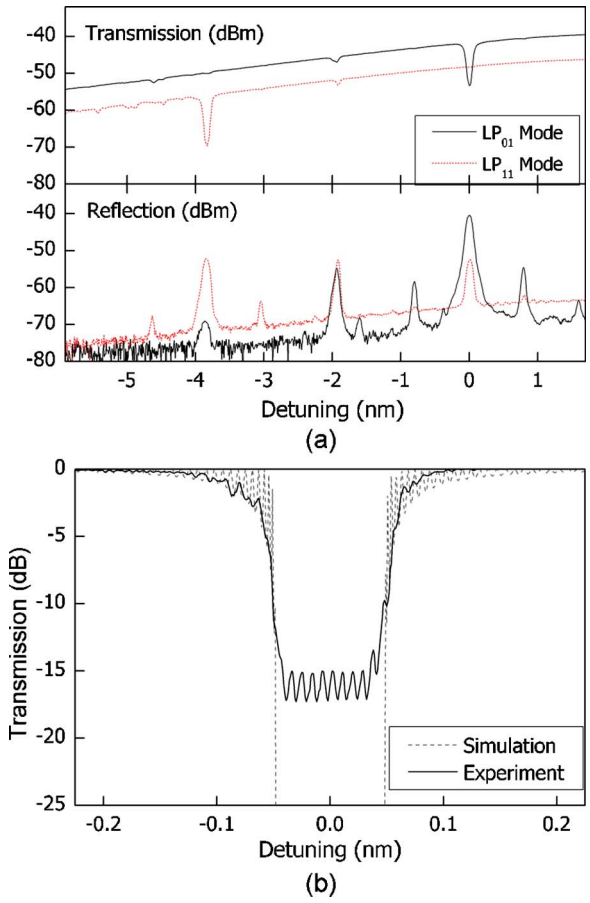

FIG. 3. (Color online) (a) Transmission and reflection spectra showing mode selectivity. (b) High-resolution (1 pm) transmission spectra including fit by transfer matrix method.

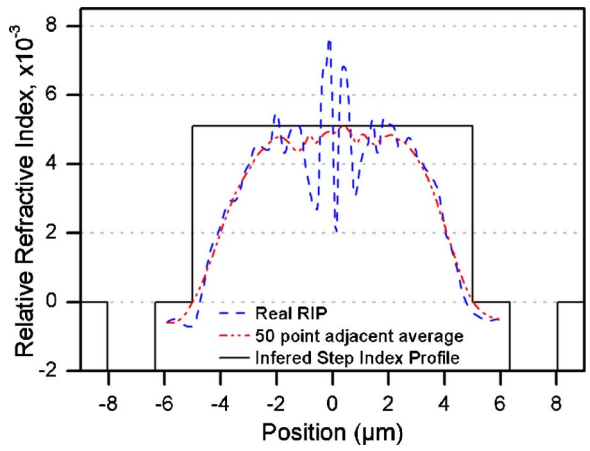

FIG. 4. (Color online) Refractive index profiles for different considerations.

III. MODELING

A difference between step-index waveguides and air-silica structured waveguides (in fact, all microstructured waveguides) is that modes are bound in step-index waveguides (assuming an infinite cladding) whereas, strictly speaking, there are no confined modes in structured waveguides because leakage loss between holes exists even when the cladding is infinite. Thus, to accurately model structured waveguides, the modeling techniques must account for confinement loss, i.e., mode leakage. Existing models relying on basis function expansions do not determine waveguide confinement loss because they do not analyze the optical field beyond the structured boundaries since it is not required to perform modal field calculations.[49] In order to address this problem, and to allow noncircular hole geometry and mode leakage, a new method, still established on the useful basis function expansion technique but with external analysis, called the "adjustable boundary condition-Fourier decomposition method (ABC-FDM)" was developed by Poladian *et al.*[49] This technique was initially applied to the scalar wave equation to obtain the best basis functions, and was subsequently extended to the vector wave equation to incorporate all properties of electromagnetic radiation.[50] The principle behind the method is to calculate the effective mode index containing an imaginary part which is related to the confinement loss through the use of a chosen basis function, in this case a harmonic Fourier decomposition that contains the adjustable boundary conditions to ensure continuation of the field into the region beyond the microstructure. The determined effective index can be reinserted into the initial process to refine the calculations leading to convergence.

To initiate the calculations, the fiber geometry was mapped. The parameters were determined from a combination of fiber end-face cross section taken from a SEM and the preform's refractive index profile converted into fiber dimensions (Fig. 4), which was previously verified from the Er^{3+} ion luminescence using fluorescence confocal microscopy.[51] To reduce the computational complexity, a step-index refractive index profile (Fig. 4, black solid line) was estimated using a 50-point adjacent-average smoothing (Fig. 4, dash-dot line) of the refractive index profile (Fig. 4, dash line). Index smoothing was performed to generate an index-profile that better represents the index for a wavelength of 1.5 μm. The step-index profile was determined from the peak of the smoothed index. The core-cladding boundary was defined where the core index reduced to the same value as silica ($\Delta n=0$). Previous investigation[35] demonstrated that this fiber can support two modes within the 1530 nm window. It is unlikely that the depressed cladding section between the holes and doped core contributes significantly since it is a fraction of the step index. Ion migration during drawing[52] was not factored into the index profile analysis when converting from preform to fiber dimensions. Some evidence exists, however, that ion mixing occurred based on fluorescence confocal microscopy for the different ions.[51]

The material indices for the different regions of the ASSF were chosen to be 1.443 for silica and 1.448 (1.443 +0.005) for the doped core at the wavelength of 1.5 μm. The doped core had a radius of 5 μm with the first ring of holes located at a radius of 6.34 μm. To estimate the number of modes which can be supported within the doped core, the V-parameter was calculated, using the step-index approximation, to be $V=2.469$ at 1.53 μm. This implies the waveguide is just above the single-mode cutoff. To compare the influence of the holey region, the mode confinement of a step-index fiber with the same dimensions was calculated (Table I). Altering the waveguide to include the structured region reduces the effective index of the higher order modes, demonstrating the additional leakage. The leakage infers that the higher order modes will interact, through additional evanescent field penetration, much more with the holes. This opens the opportunity of using the ASSF as a sensing element. The theoretical effective index difference for the higher order mode, $\Delta n_{\text{eff}}=-3.81\times10^{-3}$ (average of TM_{01}, TE_{01}, and HE_{11}) is in excellent agreement with the experimentally observed $\Delta n_{\text{eff}}=-3.8\times10^{-3}$.

TABLE I. Theoretical and experimental results of the effective indices for the modes at 1530 nm.

	Mode	n_{eff}	$\Delta n_{\text{eff}}(\times10^{-3})$	Confinement loss (dB/m)
Step-index fiber	HE_{11}	1.446 58	0	<0.01
	TM_{01}	1.443 49	−3.09	<0.01
	TE_{01}	1.443 49	−3.09	<0.01
	HE_{21}	1.443 48	−3.10	<0.01
ASSF	HE_{11}	1.446 36	0	<0.01
	TM_{01}	1.442 57	−3.79	12
	TE_{01}	1.442 54	−3.82	13.62
	HE_{21}	1.442 54	−3.82	13.17
FBG in ASSF	Fundamental, LP_{01}	1.445 6	0	n/a
	High-order, LP_{11}	1.441 8	−3.8	n/a

IV. LASING PROPERTIES

The experimental configuration used to analyze the lasing properties is shown schematically in Fig. 5. Free-space butt-coupling was used to couple selectively into either LP_{01}(pump) or LP_{11}(pump) modes. The reason the waveguide supports selective mode lasing stems from the spatial dependence of the lasing mode on the profile of the pump mode and the subsequent gain accessible to the laser modes. The higher order pump mode excites the gain region at the edges strongly compared to the center, despite the higher

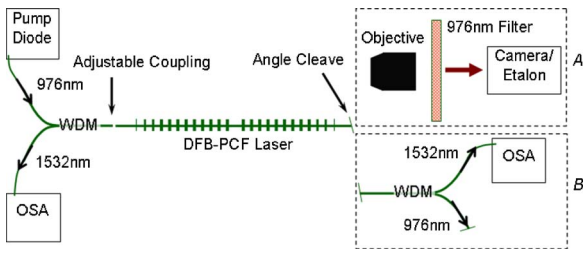

FIG. 5. (Color online) Schematic configuration for characterizing the fiber laser. Configuration A was used to study the mode shape and linewidth, B was used to study the spectra in the copumping direction.

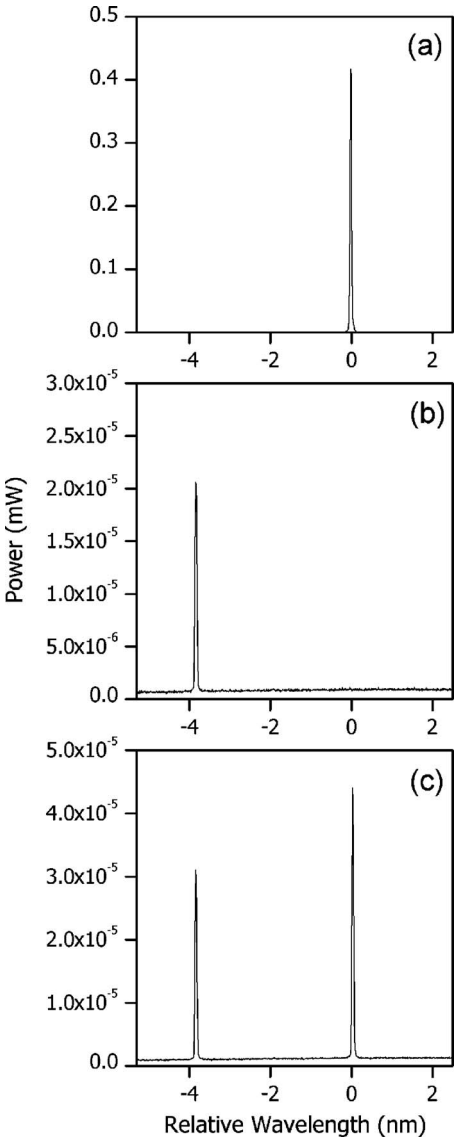

FIG. 6. Lasing spectra of (a) LP_{01}(laser); (b) LP_{11}(laser) mode; and (c) both modes, recorded on OSA.

gain in the center. For example, a LP_{01}(laser) mode is generated when the pump is launched into the LP_{01}(pump) mode, whereas a LP_{11}(laser) mode is generated when the pump is in the LP_{11}(pump) mode. In practice this distinction is less striking because the accessible gain for LP_{11}(laser) is highest at the center of the fiber and not where the peaks of the lobes are located. Monitoring of the laser spectra was performed with an optical spectrum analyzer, demonstrating the lasing of LP_{01}(laser), LP_{11}(laser), and both LP_{01}(laser) and LP_{11}(laser) simultaneously as shown in Fig. 6.

Near-field mode profiles (each normalized to their individual peaks) were captured using a Vidicon camera (sensitive from 0.4–2 μm) to examine the lasing and pump mode profiles (Fig. 7). The mode profiles were focused onto the camera using a microscope objective. The residual pump light transmitted through the fiber was attenuated to avoid detector saturation, and the influence from the DFB lasing light was ignored since the lasing power was at least an order of magnitude less than the pump power. When analyzing the laser modes the residual 976 nm light is removed using a

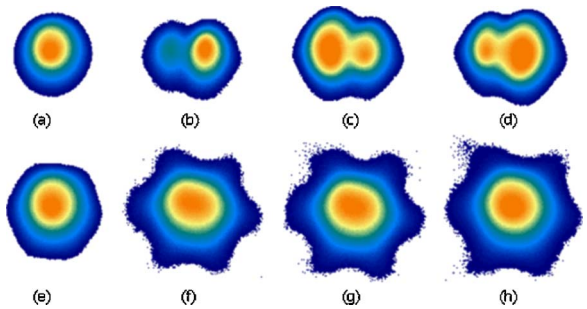

FIG. 7. (Color online) Normalized mode profiles from the DFB-PCF. Residual pump (976 nm) modes: (a) LP_{01}(pump); (c) and (e) LP_{11}(pump); and (g) both LP_{01}(pump) and LP_{11}(pump). Laser mode profiles: (b) LP_{01}(laser); (d) and (f) LP_{11}(laser); and (h) both LP_{01}(laser) and LP_{11}(laser).

high-pass filter (>1.1 μm) and the attenuator is removed. The LP_{01}(pump) [Fig. 7(a)] generates LP_{01}(laser) mode [Fig. 7(e)], whereas LP_{11}(pump) [Figs. 7(b) and 7(c)] generates LP_{11}(laser) [Figs. 7(f) and 7(g)]. The near-field image of LP_{11}(laser) differs from the expected double-peak profile because the gain accessible by LP_{11}(laser) is largest at the center of the fiber, which is accessed by the wings of the lobes. Consequently, the lasing is more dominant at this location. Another contributor may be residual ASE generated by the ASSF on either side of the DFB structure and also some minor degradation of the image from the optics. To couple into LP_{11}(pump), the coupling fiber was translated by ~4 μm from the center of the core of the DFB fiber so that it was positioned close to the edge of the doped core region. It is this large spatial offset which allows the edges of the doped region to be pumped strongly enough to overcome the higher gain seen by the fundamental mode in the center.

Dual lasing was generated by altering the pump coupling to excite both LP_{01}(pump) and LP_{11}(pump). Due to the lower threshold of LP_{01}(laser) and the greater overlap with the high gain center of the fiber, the signal was significantly stronger at this wavelength. The dual lasing profile is shown in Fig. 7(h). From the profile, it is clear that the higher order mode probes the hole structure more so than the fundamental mode.

A qualitative measurement of the relative thresholds for both lasing modes was acquired by observing the lasing spectra on the OSA and varying the pump power. The threshold values were 25 mW for LP_{01}(laser), whereas the LP_{11}(laser) required 60 mW. This clearly demonstrates the lower gain accessible for LP_{11}(laser) as well as gain competition at higher pump powers from the doped core mode. To establish LP_{11}(laser) threshold, high pump power alignment was done initially, followed by the variation in pump power. This was to ensure the optimal coupling conditions for LP_{11}(laser).

V. CONCLUSION

An alternative approach to obtaining selective lasing with improved interaction with the air holes of a structured optical fiber has been proposed and demonstrated. Dual mode lasing was obtained by selective excitation of different modes through variable launch conditions. Gain competition between lasing modes was increased by writing a grating so

that field localization in the step index leads to spatial hole burning, which in turn increases the available Er^{3+} for LP_{11} mode lasing. Previous work[45] did not report dual mode lasing because the grating was weaker and coupling conditions were not altered to excite the high-order mode—the effective index of that part of the fiber draw was also reduced by a slightly smaller outer diameter. The advantage of a laser operating on the LP_{11} mode is the increased resonant field overall with the hole for spectrally specific sensing. In this way it is plausible that a dual mode laser can operate with lasing on the LP_{01} mode as reference and the LP_{11} as signal probe. This would allow removal of environmental perturbations, such as temperature, from the sensing fiber.

Future fiber designs aim for improved performance by adjusting the distribution of rare-earth ions. For example, one approach is to create a ring distribution of dopant around an undoped core or, alternatively, surrounding a hole located at the center of the core of a Fresnel fiber laser,[31] as there appears to be sufficient gain for LP_{11}(laser) despite the limited concentration of rare-earth ions. This would permit a very sensitive fiber device, one containing a single or numerous centrally positioned holes surrounded by a ring of rare-earth ions.

ACKNOWLEDGMENTS

The authors thank Fotios Sidiroglou for supplying fluorescence confocal microscopy data[51] to assist with fiber modeling. Cicero Martelli thanks CAPES-Brasil for funding his scholarship. This work was funded by an ARC Discovery Project Grant.

[1]H. Kogelnik and C. V. Shank, Appl. Phys. Lett. **18**, 152 (1971).
[2]I. P. Kaminow, H. P. Weber, and E. A. Chandross, Appl. Phys. Lett. **18**, 497 (1971).
[3]O. Mikami, Jpn. J. Appl. Phys. **20**, L488 (1981).
[4]K. Utaka, S. Akiba, K. Sakai, and Y. Matsushima, Electron. Lett. **17**, 961 (1981).
[5]J. Canning and M. G. Sceats, Electron. Lett. **30**, 1344 (1994).
[6]A. Asseh, H. Storoy, J. T. Kringlebotn, W. Margulis, B. Sahlgren, S. Sandgren, R. Stubbe, and G. Edwall, Electron. Lett. **31**, 969 (1995).
[7]W. H. Loh and R. I. Laming, Electron. Lett. **31**, 1440 (1995).
[8]M. Sejka, P. Varming, J. Hübner, and M. Kristensen, Electron. Lett. **31**, 1445 (1995).
[9]D. Y. Stepanov, J. Canning, L. Poladian, R. Wyatt, G. Maxwell, R. Smith, and R. Kashyap, Opt. Fiber Technol. **5**, 209 (1999).
[10]J. Canning, "New Fibre and Grating Technologies for Lasers and Sensors," Invited Chapter in Frontiers, in *Lasers and Electro-Optics Research*, edited by. W. T. Arkin (Nova Science, Hauppauge, NY, 2006), and references therein.
[11]B. Poumellec, P. Guénot, I. Riant, P. Sansonetti, P. Niay, P. Bernage, and J. F. Bayon, Opt. Mater. **4**, 441 (1995).
[12]P. J. Lemaire, R. M. Atkins, V. Mizrahi, and W. A. Reed, Electron. Lett. **29**, 1191 (1993).
[13]J. Canning, M. Åslund, and P.-F. Hu, Opt. Lett. **25**, 1621 (2000).
[14]M. Åslund, J. Canning, and G. Yoffe, Opt. Lett. **24**, 1826 (1999).
[15]J. Canning, Opt. Fiber Technol. **6**, 275 (2000).
[16]J. Albert, M. Fokine, and W. Margulis, Opt. Lett. **27**, 809 (2002).
[17]N. Groothoff, J. Canning, E. Buckley, K. Lyttikainen, and J. Zagari, Opt. Lett. **28**, 233 (2003).
[18]J. Hübner, P. Varming, and M. Kristensen, Electron. Lett. **33**, 139 (1997).
[19]Z. E. Harutjunian, W. H. Loh, R. I. Laming, and D. N. Payne, Opt. Lett. **32**, 346 (1996).
[20]A. Michie and J. Canning, Postdeadline paper, in Australian Conference on Optical Fibre Technology (ACOFT 2002), Darling Harbor Sydney, Australia, 2002.
[21]J. L. Philipsen, M. O. Berendt, P. Varming, V. C. Lauridsen, J. H. Povlsen, J. Hübner, M. Kristensen, and B. Palsdottir, Electron. Lett. **34**, 678 (1998).
[22]P. Kaiser and H. W. Astle, Bell Syst. Tech. J. **53**, 1021 (1974).
[23]J. C. Knight, T. A. Birks, P. St. J. Russell, and D. M. Atkin, Opt. Lett. **21**, 1547 (1996).
[24]J. C. Knight, T. A. Birks, P. St. J. Russell, and J. P. de Sandro, J. Opt. Soc. Am. A **15**, 748 (1998).
[25]J. Canning, Opt. Commun. **176**, 121 (2000).
[26]P. Yeh, A. Yariv, and E. Maron, J. Opt. Soc. Am. **68**, 1196 (1978).
[27]R. F. Cregan, B. J. Mangan, J. C. Knight, T. A. Birks, P. St. J. Russell, P. J. Roberts, and D. C. Allan, Science **285**, 1537 (1999).
[28]J. Broeng, S. E. Barkou, T. Sondergaard, and A. Bjarklev, Opt. Lett. **25**, 96 (2000).
[29]S. G. Johnson, M. Ibanescu, M. Skorobogatiy, O. Weisberg, T. D. Engeness, M. Soljacic, S. A. Jacobs, J. D. Joannopoulos, and Y. Fink, Opt. Express **9**, 748 (2001).
[30]J. Canning, Opt. Commun. **207**, 35 (2002).
[31]J. Canning, E. Buckley, and K. Lyytikainen, Opt. Lett. **28**, 230 (2003).
[32]A. Bjarklev, J. Broeng, S.E. Barkou and K. Dridi, in ECOC '98, Madrid, September 1998.
[33]A. Ortigosa-Blanch, J. C. Knight, W. J. Wadsworth, J. Arriaga, B. J. Mangan, T. A. Birks, and P. St. J. Russell, Opt. Lett. **25**, 1325 (2000).
[34]A. Michie, J. Canning, K. Lyytikainen, M. Åslund, and J. Digweed, Opt. Express **12**, 5160 (2004).
[35]C. Martelli, J. Canning, N. Groothoff, and K. Lyytikainen, Opt. Lett. **30**, 1785 (2005).
[36]H. R. Sørensen, J. Canning, J. Lægsgaard, and K. Hansen, Opt. Express **14**, 6428 (2006).
[37]Y. L. Hoo, W. Jin, H. L. Ho, D. N. Wang, and R. S. Windeler, Opt. Eng. **41**, 8 (2002).
[38]J. M. Fini, Meas. Sci. Technol. **15**, 1120 (2004).
[39]J. B. Jensen, L. H. Pedersen, P. E. Hoiby, L. B. Nielsen, T. P. Hansen, J. R. Folkenberg, J. Riishede, D. Noordegraaf, K. Nielsen, A. Carlsen, and A. Bjarklev, Opt. Lett. **29**, 1974 (2004).
[40]K. P. Hansen, Opt. Express **11**, 1503 (2003).
[41]B. J. Eggleton, P. S. Westbrook, R. S. Windeler, S. Spälter, and T. A. Strasser, Opt. Lett. **24**, 1460 (1999).
[42]T. Søndergaard, J. Lightwave Technol. **18**, 589 (2000).
[43]A. Cucinotta, F. Poli, S. Selleri, L. Vincetti, and M. Zoboli, J. Lightwave Technol. **21**, 782 (2003).
[44]J. Canning, N. Groothoff, E. Buckley, T. Ryan, K. Lyttikainen, and J. Digweed, Opt. Express **11**, 1995 (2003).
[45]N. Groothoff, J. Canning, T. Ryan, K. Lyytikainen, and H. Inglis, Opt. Express **13**, 2924 (2005).
[46]W. G. French, J. B. MacChesney, P. B. O'Conner, and G. W. Tasker, Bell Syst. Tech. J. **53**, 951 (1974).
[47]E. Delevaque, T. Georges, M. Monerie, P. Lamouler, and J. F. Bayon, IEEE Photonics Technol. Lett. **5**, 73 (1993).
[48]M. Åslund, Ph.D. thesis, The University of Sydney, 2004.
[49]L. Poladian, N. A. Issa, and T. M. Monro, Opt. Express **10**, 449 (2002).
[50]N. A. Issa, and L. Poladian, J. Lightwave Technol. **21**, 1005 (2003).
[51]F. Sidiroglou (private communication).
[52]K. Lyytikäinen, S. T. Huntington, A. L. G. Carter, P. McNamara, S. Fleming, J. Abramczyk, I. Kaplin, and G. Schötz, Opt. Express **12**, 972 (2004).